Fast Dynamic Walking with RH5 Humanoid Robot

Ivan Bergonzani[1], Mihaela Popescu[2], Shivesh Kumar[1,3] and Frank Kirchner[1,2]

***Abstract*— Humanoid robots have the potential of becoming general purpose robots augmenting the human work-force in industries. However, they must match the agility and versatility of humans. It is particularly challenging for humanoids actuated with electric drives to achieve that as one must strive for the right balance between mass-inertial distribution in the robot as well as velocity and force transmissions in its actuation concept. In addition to optimal design of the robot, the control system must be designed to exploit the full potential of the robot. In this paper, we perform experimental investigations on the dynamic walking capabilities of a series-parallel hybrid humanoid named RH5. We demonstrate that it is possible to walk up to speeds of 0.43 m/s with a position controlled robot without full state feedback which makes it one of the fastest walking humanoids with similar size and actuation modalities. Video of the experiments is available at: https://youtu.be/39GL2vPedGY**

I. INTRODUCTION

Humanoid robots can be employed in a wide range of applications, from search and rescue missions to industrial environments and tasks in spaces specifically designed for humans. Due to their versatility and the broad range of possible use cases, humanoid robots will play an important role in the future of technological progress. To enable this, humanoid robotics research is striving to achieve the agility of humans. In this context, recent developments show an increased interest in achieving fast and dynamic bipedal walking. In addition to advances in controls, the performance of humanoid walking is highly dependent on hardware design, e.g. actuation type, leg kinematics and robot size.

Early on, bipedal walking developments have been made in the class of medium-sized humanoid robots under 1.25 m height, such as the ASIMO [1] robot from Honda introduced in the year 2000, followed by the humanoid robot HUBO [2] released by KAIST in 2005. Currently, Atlas [3] from Boston Dynamics is one of the most advanced and dynamic full scale humanoids. In contrast to electrically powered humanoid robots, its athletic capabilities are enabled by hydraulic drives that provide high force and velocity transmissions needed to execute such motions. Furthermore, the bipedal robot Cassie [4] and its full humanoid version Digit [5] developed by Agility Robotics achieved high walking performance by leveraging a leg design inspired from bird walking mechanism and employing cycloidal drives, which display higher dynamics as compared to harmonic drives but also leads to smaller humanoids.

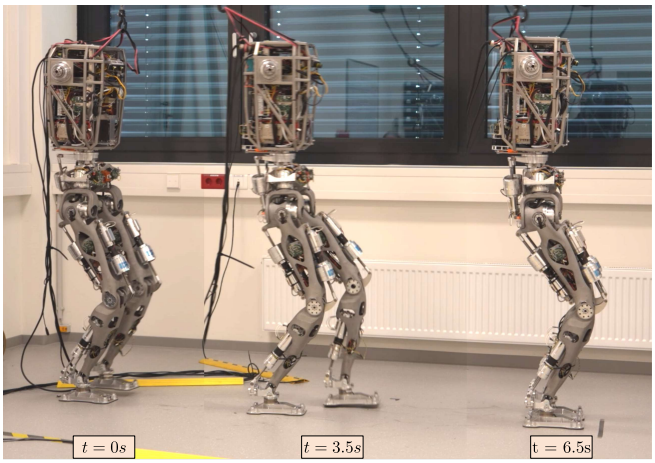

Fig. 1: The RH5 humanoid robot lower body performing a fast dynamic walk with a measured speed of 0.43 m/s (verified with motion capture system).

Our focus lies on full scale humanoid robots powered by electric drives, whose walking speed is still limited. To the best of the author's knowledge, most humanoids in active research have documented walking speeds of less than 0.5 m/s in practical experiments with real robots as shown in Table I. The highest speed has been achieved by the humanoid robot Lola [6], which performed fast walking up to 0.92 m/s by taking advantage of active toe joints in order to execute long strides. DARPA robotics challenge winner DRC-Hubo+ [7] reaches a walking velocity of 0.44 m/s in experimental setup [8] and can go up to 0.5 m/s according to the specifications. Moreover, the humanoid Toro [9] achieved a velocity of 0.37 m/s in torque control, while HRP-2 [10] obtained long strides of 100 cm and a speed of $\sim$0.33 m/s. The robot Talos [11] reached a speed of 0.25 m/s in torque control by modeling the hip flexibility. The robots SURENA IV [12] and JAXON [13] have obtained lower walking speeds under 0.20 m/s. Moreover, humanoids with series elastic actuators such as Valkyrie [14] and WALK-MAN [15] have slower speeds in walking experiments, since their main focus is robustness to operate in damaged human-engineered environments and lift heavy weights.

In this paper, we present an experimental evaluation of the dynamic capabilities of the RH5 humanoid robot lower body performing for the first time a dynamic walk up to 0.43 m/s as shown in Fig. 1. Excluding robots with active toe joints, RH5 is among the fastest humanoids with similar size

[1] Robotics Innovation Center, German Research Center for Artificial Intelligence (DFKI GmbH), 28359 Bremen, Germany. ivan.bergonzani@dfki.de
[2] Robotics Group, Faculty of Mathematics and Computer Science, University of Bremen, 28359 Bremen, Germany.
[3] Division of Dynamics, Department of Mechanics & Maritime Sciences, Chalmers University of Technology, Gothenburg, Sweden.

TABLE I: Overview of walking speed measured in experimental scenarios of full size humanoid robots with electric drives, where t_{ss} and t_{ds} represent the duration of the single and double support phases, HD stands for harmonic drive and SEA stands for series elastic actuator. The velocities preceded by $\sim$ are approximated from data plots in the cited references.

Robot	Manufacturer	Height [m]	Mass [kg]	Speed [m/s]	Step [m]	t_{ss} [s]	t_{ds}[s]	Drive
Lola [6]	TU Munich, Germany	1.80	55	0.92	0.65	0.7	-	HD
DRC-Hubo+ [8]	KAIST, South Korea	1.70	80	0.44	0.40	0.9	-	HD
Toro [9]	DLR, Germany	1.74	76	0.37	0.55	1.1	0.4	HD
HRP-2 [10]	Kawada Industries and AIST, Japan	1.60	65	$\sim$ 0.33	0.50	$\sim$ 1.5	-	HD
Talos [11]	PAL Robotics, Spain	1.75	95	0.25	0.35	1.2	0.2	HD
SURENA IV [12]	University of Tehran, Iran	1.70	68	0.19	-	-	-	HD
JAXON [13]	University of Tokyo, Japan	1.88	127	$\sim$ 0.08	$\sim$ 0.10	$\sim$ 0.8	-	HD
Valkyrie [14]	NASA, USA	1.87	129	0.08	0.25	1.5	1.5	SEA
WALK-MAN [15]	IIT, Italy	1.91	132	0.03	0.05	1.2	0.3	SEA

and actuation modalities. Moreover, the dynamic abilities of RH5 are demonstrated in further experiments of fast stepping in place and long walking stride. These results have been achieved by combining zero-moment point motion planning and whole body control approaches in a tailored manner which is suitable for achieving a high performance from position controlled robots without full state feedback.

Organization: The paper is structured as follows. Section II introduces the humanoid robot RH5 and the implemented control stack. Section III describes the experimental setup, while in Section IV we present and evaluate the obtained results. In Section V we draw the conclusions and discuss future work.

II. METHODOLOGY

This section explains the methodology employed in this paper starting with the robot description, motion planning approach, considerations for a position controlled system and task space inverse dynamics based whole body control. An overview of the control scheme is shown in Fig. 3.

A. RH5 Robot

RH5 [16] is a 2 m tall series-parallel hybrid humanoid robot developed by the DFKI Robotics Innovation Center with 32 degrees of freedom (DoFs) and a weight of 62.5 kg. The robot has 6 DoFs per leg, 7 DoFs on each arm, 3 DoFs for the body and 3 DoFs for the head. The design of RH5 consists of serial and parallel actuation mechanisms. In particular, ankles and wrists mechanisms consist of two parallel linear actuators that account for roll and pitch rotation. Moreover, the robot is powered by electric actuators with harmonic drives. Due to the single stage reduction ratio and low backlash, they provide high torques while being precise and rigid. The robot is also equipped with an inertial measurement unit, joint encoders, and force-torque (F/T) sensors. The mass-inertial distribution of RH5 arms was not optimal (see Fig. 2 left) which caused difficulties in generating stable walking behavior. An improved upper body design of this robot, called RH5 Manus [17] (see Fig. 2 right) has optimal mass-inertial distribution close to a human arm and is capable of performing dynamic movements such as weight lifting [18], boxing and even dancing [19].

Fig. 2: The lower body of the RH5 humanoid (left) will be combined with the new upper body robot RH5 Manus (right).

In this work, RH5 has been tested in a configuration without head and arms to evaluate the dynamic capabilities of the lower body as we intend to combine the lower body of RH5 humanoid with RH5 Manus in the near future.

B. Motion Planner

The motion planning for the RH5 humanoid is done in two stages: 1) compute footstep and Zero Moment Point (ZMP) plan with a joystick input, and 2) compute the optimal center of mass (CoM) trajectory with the planned ZMP reference (also referred to as walking pattern generation problem).

1) Footstep and ZMP Planner: The motion controller receives the desired velocity and direction from a joystick. Using this input, a footstep plan is created and used to define a ZMP trajectory based on cubic (zero-order hold) piecewise polynomials with its knot points inside the support polygon of the feet. The footstep planner provides only 2 steps in advance, namely one to move forward and one to stop. The final pose of the swing foot at the end of the step is based from the anchor foot pose and the received input.

2) CoM Trajectory Planner: Using a linear inverted pendulum model (LIPM) we compute an optimal CoM trajectory as in [20]. Considering a constant CoM height c_z and gravity

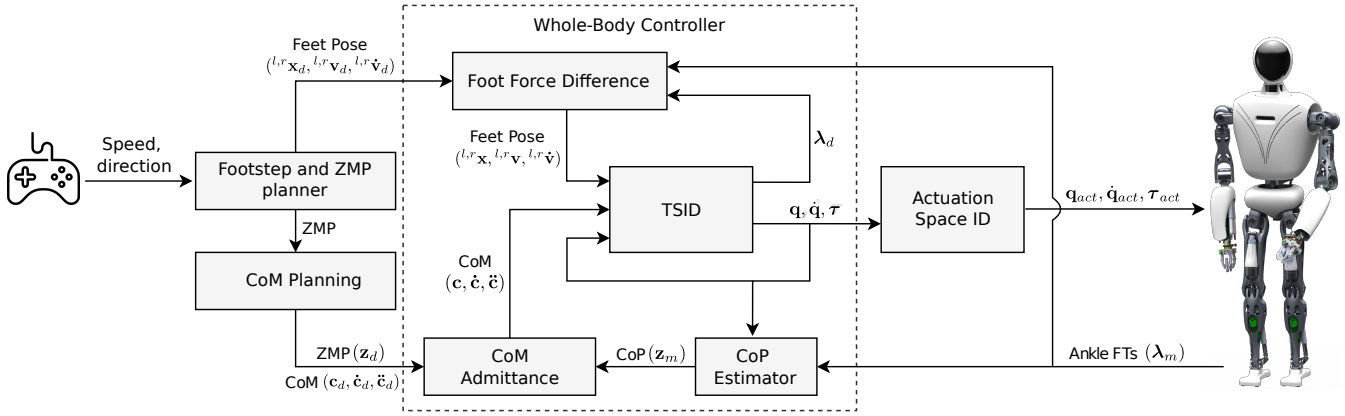

Fig. 3: Control scheme implemented for the experiments. RH5 is controlled in position. TSID acceleration output is double integrated to get independent joint space references $\mathbf{q}, \dot{\mathbf{q}}, \boldsymbol{\tau}$, then transformed in actuation space positions $\mathbf{q}_{act}, \dot{\mathbf{q}}_{act}, \boldsymbol{\tau}_{act}$.

constant g, the LIPM dynamics can be written in the form:

$$\begin{aligned}\dot{\mathbf{x}} &= \mathbf{A}\mathbf{x} + \mathbf{B}\mathbf{u} = \begin{bmatrix} 0_{2\times2} & \mathbb{I}_{2\times2} \\ 0_{2\times2} & 0_{2\times2} \end{bmatrix} \mathbf{x} + \begin{bmatrix} 0_{2\times2} \\ \mathbb{I}_{2\times2} \end{bmatrix} \mathbf{u} \\ \mathbf{y} &= \mathbf{C}\mathbf{x} + \mathbf{D}\mathbf{u} = \begin{bmatrix} \mathbb{I}_{2\times2} & 0_{2\times2} \end{bmatrix} \mathbf{x} - \frac{c_z}{g}\mathbb{I}_{2\times2}\mathbf{u} \end{aligned} \tag{1}$$

where $\mathbf{x} = [c_x, c_y, \dot{c}_x, \dot{c}_y]$ represents the system state formed by CoM position and velocity in the horizontal plane, $\mathbf{u} = [\ddot{c}_x, \ddot{c}_y]$ is the control variable (CoM acceleration) and the system output $\mathbf{y} = [z_x, z_y]$ is the corresponding ZMP. In order to obtain the optimal CoM, it is possible to solve a continuous time varying LQR problem subject to the LIPM dynamics (1) and defined by the value function:

$$V(\mathbf{x}, t_i) = \min_{\mathbf{u}[t_i:t_f]} \bar{\mathbf{x}}(t_f)^T \mathbf{S}\bar{\mathbf{x}}(t_f) + \int_{t_i}^{t_f} \bar{\mathbf{y}}^T \mathbf{Q}_\mathbf{y}(\bar{\mathbf{y}}) + \mathbf{u}^T \mathbf{R}\mathbf{u}\, dt$$

where state $\bar{\mathbf{x}} = [\mathbf{c} - \mathbf{y}_d(t_f); \dot{\mathbf{c}}]$ and observation variables $\bar{\mathbf{y}} = \mathbf{y} - \mathbf{y}_d(t_f)$ are expressed with respect to the final condition on ZMP. Weighting matrix $\mathbf{Q}_\mathbf{y}$ defines the importance of ZMP tracking while matrix $\mathbf{R}$ penalizes CoM accelerations. Since we are not using any feedback on the CoM, differently from the original paper [20] we don't use online stabilization of the CoM trajectory but instead we compute the nominal CoM trajectory once and track it blindly.

C. Considerations for a Position Controlled Robot

Since the joints are position controlled, the robot motion can be very stiff. In order to reduce and absorb impact forces with the ground, we use additional stabilization methods that act on the desired trajectory references as in [21]. More specifically, we use CoM admittance [22] and Foot Force difference [23]. Both of them require measurements from the F/T sensors placed at the ankles, which is the only feedback from the robot used in this work.

1) CoM admittance: The purpose of CoM admittance is to make the robot follow external perturbations instead of counteracting them, absorbing external wrenches and eventual oscillations that they might generate. To accomplish this, the center of mass is accelerated proportionally to the error between the measured center of pressure $\mathbf{z}_m$ and the desired ZMP $\mathbf{z}_d$ (equivalent to the center of pressure on flat surfaces) in the world frame. The resulting CoM acceleration $\ddot{\mathbf{c}}$ is defined as follows:

$$\begin{aligned}\ddot{\mathbf{c}} &= \ddot{\mathbf{c}}_d + {}^w\mathbf{R}_b \mathbf{A}_c {}^w\mathbf{R}_b^T (\mathbf{z}_m - \mathbf{z}_d) \\ \mathbf{A}_c &= \begin{bmatrix} A_{c,x} & 0 & 0 \\ 0 & A_{c,y} & 0 \\ 0 & 0 & 0 \end{bmatrix}\end{aligned} \tag{2}$$

where $\ddot{\mathbf{c}}_d$ represents the desired CoM acceleration, $\mathbf{A}_c$ is the compliance gain matrix on the horizontal plane expressed in robot body frame and ${}^w\mathbf{R}_b$ accounts for the yaw rotation from world frame to robot body frame.

In order to avoid drifting from the desired CoM position and velocity, the corresponding references are changed accordingly based on the controller time step t:

$$\begin{aligned}\mathbf{c} &= \mathbf{c}_d + {}^w\mathbf{R}_b \mathbf{A}_c {}^w\mathbf{R}_b^T (\mathbf{z}_m - \mathbf{z}_d)\, t^2 \\ \dot{\mathbf{c}} &= \dot{\mathbf{c}}_d + {}^w\mathbf{R}_b \mathbf{A}_c {}^w\mathbf{R}_b^T (\mathbf{z}_m - \mathbf{z}_d)\, t\end{aligned} \tag{3}$$

2) Foot Force difference: Using foot force admittance, the robot is able to anticipate late contacts with the ground and absorb early contacts as well as impacts from other external sources. Differently from [21], the stabilization is implemented with respect to the force distribution instead of absolute force measurements. We compute a force distribution quantity Δ as:

$$\Delta = \frac{{}^l f_m^z}{({}^l f_m^z + {}^r f_m^z)} - \frac{{}^l f_d^z}{({}^l f_d^z + {}^r f_d^z)} \tag{4}$$

where ${}^l f_m^z$ and ${}^r f_m^z$ are the z-axis forces measured at the left and right ankles FT sensors ($\boldsymbol{\lambda}_m$), ${}^l f_d^z$ and ${}^r f_d^z$ are the desired respective forces from the inverse dynamics solver TSID ($\boldsymbol{\lambda}_d$). Along the world z-axis, the left foot velocity ${}^l v^z$ and right foot velocity ${}^r v^z$ are updated as follows:

$$\begin{aligned}{}^l v^z &= {}^l v_d^z + K_f \Delta \\ {}^r v^z &= {}^r v_d^z - K_f \Delta\end{aligned} \tag{5}$$

where ${}^l v_d^z$ and ${}^r v_d^z$ are the left and right foot velocities corresponding to the desired trajectory, and K_f is the gain modulating the compliance.

Similarly, z-component of left and right feet positions $({}^l x^z, {}^r x^z)$ and accelerations $({}^l \dot{v}^z, {}^r \dot{v}^z)$ references are also changed based on the controller time step t to improve tracking and avoid excessive drifting from the desired position:

$$\begin{aligned} {}^l x^z &= {}^l x_d^z + K_f \Delta t \\ {}^r x^z &= {}^r x_d^z - K_f \Delta t \end{aligned} \tag{6}$$

$$\begin{aligned} {}^l \dot{v}^z &= {}^l \dot{v}_d^z + \frac{K_f \Delta}{t} \\ {}^r \dot{v}^z &= {}^r \dot{v}_d^z - \frac{K_f \Delta}{t} \end{aligned} \tag{7}$$

D. Whole-Body Controller

In order to make RH5 follow the desired motion we used a Task Space Inverse Dynamics (TSID [24]) based Whole-Body Controller (WBC), therefore solving at each control update the following quadratic programming (QP) problem:

$$\min_{\ddot{\mathbf{q}}, \boldsymbol{\lambda}, \boldsymbol{\tau}} \quad \sum_i \alpha_i \|\mathbf{J}_i \ddot{\mathbf{q}} + \dot{\mathbf{J}}_i \dot{\mathbf{q}} - \dot{\mathbf{v}}\|_2 \tag{8a}$$

$$\text{s.t.} \quad \mathbf{M}(\mathbf{q})\ddot{\mathbf{q}} + \mathbf{b}(\mathbf{q}, \dot{\mathbf{q}}) = \boldsymbol{\tau} + \mathbf{J}_c^T \boldsymbol{\lambda} \tag{8b}$$

$$\mathbf{J}_{c,j} \ddot{\mathbf{q}} = -\dot{\mathbf{J}}_{c,j} \dot{\mathbf{q}}, \quad \forall j \tag{8c}$$

$$\mathbf{U}_j \boldsymbol{\lambda}_j = 0, \, \forall j \tag{8d}$$

$$\mathbf{l}_m (\mathbf{q}, \dot{\mathbf{q}}) \leq \ddot{\mathbf{q}} \leq \mathbf{l}_M (\mathbf{q}, \dot{\mathbf{q}}) \tag{8e}$$

$$\boldsymbol{\tau}_m \leq \boldsymbol{\tau} \leq \boldsymbol{\tau}_M \tag{8f}$$

with decision variables including joint accelerations $\ddot{\mathbf{q}}$, joint torques $\boldsymbol{\tau}$, and contact wrenches $\boldsymbol{\lambda} = (m^x, m^y, m^z, f^x, f^y, f^z)^T \in \mathbb{R}^6$. The cost function (8a) consist of a weighted sum of Cartesian tracking costs which maps the cartesian reference to joint accelerations $\ddot{\mathbf{q}}$ via frame Jacobians $\mathbf{J}_i$. Tasks are weighted by scalar values α_i. The solution must satisfy the robot's equations of motion (EoM) (8b), in which $\mathbf{M}(\mathbf{q})$, $\mathbf{b}(\mathbf{q}, \dot{\mathbf{q}})$ and $\mathbf{J}_c(\mathbf{q})$ are respectively the robot's mass-inertia matrix, the bias centrifugal-Coriolis-gravity term, and the stacked Jacobian matrix relative to the contact frames. Moreover, for each contact j the QP formulation includes a zero-acceleration constraint (8c) as well as a friction cone constraint (8d) defined by the wrench friction cone matrix $\mathbf{U}_j$. Joint accelerations are constrained (8e) in such a way that when integrated over the current positions and velocities, these will not exceed their limits. Torques (8f) are also subject to their respective box limits.

Acceleration references $\dot{\mathbf{v}}$ for each Cartesian task are computed from a PD controller in the form:

$$\dot{\mathbf{v}} = \dot{\mathbf{v}}_d + \mathbf{K}_d(\mathbf{v}_d - \mathbf{v}) + \mathbf{K}_p \mathbf{e}(\mathbf{x}_d, \mathbf{x}) \tag{9}$$

where $\mathbf{x}_d, \mathbf{v}_d, \dot{\mathbf{v}}_d$ are respectively the desired position, velocity and acceleration defining the trajectory to follow. Term $\mathbf{e}(\mathbf{x}_d, \mathbf{x})$ defines the error between the two elements of the underlying matrix Lie group defining the Cartesian task. Gains $\mathbf{K}_p = K_p \mathbf{I}_{m \times m}$ and $\mathbf{K}_d = K_d \mathbf{I}_{m \times m}$ are diagonal matrices which define the correction for position and velocity errors with m being the number of task dimensions. The joint acceleration output is integrated twice to get the instantaneous joint positions $\mathbf{q}$ and velocities $\dot{\mathbf{q}}$ to be used as state for the next control step, since we do not rely on any floating base or joint feedback.

The QP problem in (8) is formulated in the generalized coordinates (in particular, the independent joint space) of the corresponding tree-type model of the robot neglecting the description of kinematic closed loops. In this way, we are able to run the control loop at 1 KHz [1]. Therefore, before sending a command to the robot, the solution $(\mathbf{q}, \dot{\mathbf{q}}, \ddot{\mathbf{q}}, \boldsymbol{\tau})^T$ has to be transformed in the actuation space using the Hybrid Robot Dynamics (HyRoDyn) [26], obtaining the corresponding actuator position, velocities and efforts which are then sent to the low level cascaded position-velocity-effort controllers on the robot.

TABLE II: Overview of the dynamic walk experiments denoted by S for slow walking and F for fast walking.

Gait Parameters	Dynamic Walk Experiments					
	S1	S2	S3	F1	F2	F3
stride [m]	0.4	0.5	0.6	0.4	0.5	0.6
t_{ss} [s]	0.8	0.8	0.8	0.6	0.6	0.6
t_{ds} [s]	0.2	0.2	0.2	0.1	0.1	0.1
speed [m/s]	0.2	0.25	0.3	0.285	0.357	0.428

III. EXPERIMENTAL DESIGN

The experimental investigation of RH5 dynamic capabilities consists of three different walking experiments.

- In the first set of tests, we show the stability and speed of the dynamic locomotion behavior. RH5 walks in a straight line from one side of the room to the other for a distance of about 2 m due to the crane limitation. The execution is repeated multiple times varying gait parameters such as step stride (e.g. distance traveled by feet during full swings), single support time t_{ss} and double support time t_{ds}. We design the experiment in such a way to test the robot on slower and on faster motions using the parameters shown in Table II.
- In a second experiment, RH5 walks in place with different variations of step height and step time, testing speed limits of the leg design. More in detail, we tested several combinations of step height varying from 0.04 to 0.12 meters (in increments of 0.02 m) and step time changing from 1.0 to 0.7 seconds.
- Finally, we test the robot using a walking pattern with longer stride reaching the limitation of the robot's kinematics and motion controller.

Motion trajectories are generated as described in Section II-B. During the execution of each step, we check if the user is sending any input to the robot and, in that case, the footstep plan is updated by replacing the last step with two additional steps. ZMP and CoM trajectories are updated accordingly.

[1]As shown in [25], while solving the QP directly in the actuation space enables better exploitation of robot's actuation limits, it negatively affects the control loop frequency due to the added model complexity.

TABLE III: Specification of the Whole-Body Controller (a) task parameters and (b) admittance parameters.

(a) WBC gains.

Gain	Task		
	CoM	Feet (L&R)	Torso
K_p	30	30	30
α	1000	100	10

(b) Admittance gains.

$A_{c,x}$	$A_{c,y}$	K_f
10^{-5}	3×10^{-5}	3

In order to stabilize the walking behaviors we use $SE(3)$ tasks for feet tracking, $SO(3)$ task for torso orientation and a center of mass task with constant height. Whenever a foot has to be in contact with the ground, we add a plane contact constraint to avoid any further motion. This is removed once the foot enters the swing phase. Weights and gains for each task in the WBC formulation are reported in Table IIIa, while the derivative gains are computed as $K_d = 2\sqrt{K_p}$. Moreover, the gains for the CoM admittance and Foot Force difference compliance are provided in Table IIIb.

Motion planning approach is implemented using DRAKE C++ library [27]. Behaviors and controller have been implemented using the *inria_wbc*[2] framework. Actuation space inverse dynamics is performed using the HyRoDyn library [26], while runtime execution is done inside a Orocos RTT task as part of the RoCK [28] software framework which runs on the robot's main control PC. The motion controller is running with a frequency of 1kHz.

In order to validate the walking performance of RH5, we measure the feet' ground truth poses using reflective markers placed on the robot's feet, tracked by 3 Qualisys motion capture cameras during the experiments. We then use the feet' ground truth poses and F/T sensor measurements to estimate the robot's center of pressure. Due to limited workspace and cameras' field of view, we do not report results for motions including rotation. However, the execution of rotational motions can be seen in the published video.

IV. RESULTS AND DISCUSSION

A. Dynamic Walk

After testing different gaits presented in Table II, we found that RH5 was able to successfully complete all of them. For slower motions, the walking behavior is stable, with small deviations from the desired path. While performing faster steps, RH5 is still stable but tends to lose the initial orientation because of sliding between the feet and the ground. Footsteps and estimated CoP for various experiments are shown in Fig. 4. This slipping problem can be due to the fact that the motion controller doesn't include any strategy to reduce yaw angular momentum as in [29]. Once the upper part of the robot will be upgraded, we plan to implement such method via arms swinging.

The main issue while performing dynamic walking was early contact with the ground. However, the controller is able to absorb these impacts up to some extent due to the

[2]https://github.com/resibots/inria_wbc

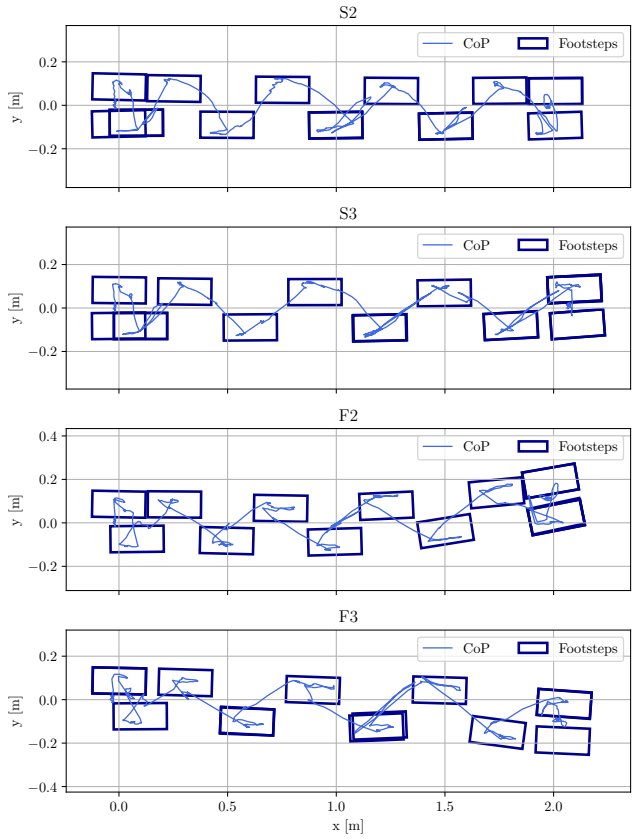

Fig. 4: Measured footsteps pose and estimated CoP trajectory for slow walking experiments (S2, S3) on the top and fast walking experiments (F2, F3) on the bottom.

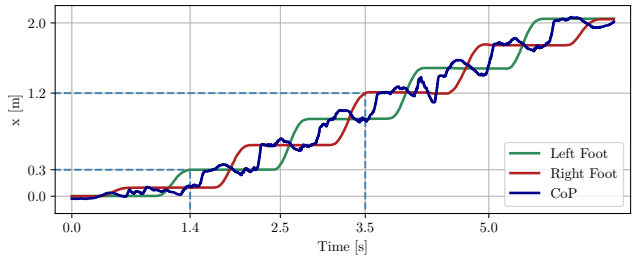

Fig. 5: Measured feet position and estimated CoP trajectory for the fastest walk experiment (F3) with a ground truth velocity of 0.43 m/s obtained with motion capture.

CoM admittance and Foot Force difference compliance. We attribute this problem to an imperfect modeling of the robot, with differences between the real and simulated one.

From motion capture feedback, the evaluated speed of the robot during the fastest gait (F3) is 0.433 m/s, slightly larger than the commanded velocity of 0.428 m/s. Fig. 5 shows a time-series of the feet positions and estimated CoP. From measured data, RH5 appears to keep double support longer than expected and executes the swing phase faster than desired. This may be caused by imperfect feet tracking and contact timings, when one foot reaches the ground too early

	Limit	Body 1	Body 2	BodyYaw	L Hip1	L Hip2	L Hip3	L Knee	L Ankle 1	L Ankle 2	R Hip1	R Hip2	R Hip3	R Knee	R Ankle 1	R Ankle 2
WALK (S2)	P	41.3	42.4	9.8	2.2	28.4	46.1	39.4	61.1	53.4	2.2	22.5	46.8	37.5	53.2	57.7
FAST WALK (F3)	P	33.3	36.6	12.0	2.7	27.2	36.4	36.4	69.7	67.3	2.7	21.2	36.7	37.3	68.4	71.8
WALK IN PLACE	P	26.0	29.9	3.6	0.9	30.7	30.3	39.2	56.8	54.3	1.0	25.2	30.6	37.8	54.6	55.6
LONG STRIDE	P	82.5	86.9	27.5	6.5	47.3	58.0	67.1	90.0	73.2	6.7	39.8	58.1	68.7	72.1	85.6
WALK (S2)	S	30.1	30.1	6.2	9.9	14.1	65.8	103.6	59.7	62.8	9.7	15.0	63.6	102.5	60.0	59.4
FAST WALK (F3)	S	33.6	33.4	9.1	15.5	14.8	97.5	111.9	73.5	74.5	14.9	13.9	92.7	111.0	78.8	72.9
WALK IN PLACE	S	29.0	30.5	2.1	3.5	17.1	31.5	111.2	42.1	41.0	4.2	16.7	33.3	110.4	42.9	41.3
LONG STRIDE	S	29.7	28.2	6.2	9.4	15.2	65.2	97.9	50.6	45.6	9.6	15.4	50.3	96.8	53.7	48.5
WALK (S2)	E	18.3	24.9	20.8	11.1	67.0	11.5	17.0	66.3	66.2	14.1	67.5	10.2	18.5	66.2	57.7
FAST WALK (F3)	E	17.5	29.8	37.3	31.9	46.8	19.5	30.5	65.7	66.3	33.1	63.5	21.3	22.6	66.4	66.4
WALK IN PLACE	E	21.8	27.8	12.4	11.1	66.3	8.1	29.3	65.2	56.8	8.6	67.3	7.4	22.2	66.3	57.8
LONG STRIDE	E	17.6	21.7	23.9	16.7	67.9	22.3	19.6	40.9	66.1	16.7	69.8	11.1	20.3	66.2	43.6

TABLE IV: Maximum percentage of use in terms of joint position (P), speed (S) and effort (E) during different experiments. For what concerns position (P) values, the percentage refers to half of the range of motion (centered in the middle point). For example, if we reached 90% in position it means that the joint was at 5% of the total range of motion (ROM) from the limit (positive or negative). WALK IN PLACE experiment has step height of 0.08m with one step every 0.75s (t_{ss}: 0.7s, t_{ds}: 0.05s). Velocities values are filtered using a low pass butterworth filter. Position and effort measurements are raw.

TABLE V: ROM of linear actuators of the RH5 robot.

Actuator	Pitch (mm)	ROM (mm)	Max. force (N)	Max. vel. (m/s)
Torso	5	195–284	2716	0.291
Hip3	5	272–431	4740	0.175
Knee	4	273–391	5845	0.140
Ankle	2	221–331	2000	0.265

(slightly bouncing back) or late. Nevertheless, the overall time for each step remains unchanged.

In Table IV we included an analysis on the actuators usage during the execution of different gaits. In both slow (S2) and fast (F3) dynamic walks, RH5 didn't reach position, velocity or effort limits for all joints except for knee joints. Table V reports specifications for the linear actuators. During the fastest walk (F3), linear actuators for hip pitch (Hip3) approached the velocity limit but used a small part of the maximum available effort which shows that the robot is over-designed for high load carrying capacity. Therefore, there is room for improvement by changing the ball screw pitches of Hip3 and Knee joints. For example, by doubling the ball screw pitches of these joints, the maximum available linear velocities will increase by a factor of two and the maximum effort available will be halved. This is still an acceptable choice as we are far from reaching the effort limits (e.g. 21.3% for right Hip3 joint and 30.5% for left Knee joint).

Regarding the effort limits, it should be considered that we are not using the full humanoid but a version with a simplified upper body. The mass difference of 14.5 kg caused by the absence of arms (12.5 kg) and head (2kg) accounts for 23% from the robot's total mass. As shown in Table IV, the effort limits stay below 77% with some margin. Even though this is not a 1:1 comparison, this result suggests that this motion will be possible even when the robot will be upgraded with the newer full upper body. Moreover, the obtained results on effort are computed on unfiltered measurements to avoid removing peaks caused by impacts with the ground, as visible in Fig. 6 around 5 seconds into the experiment.

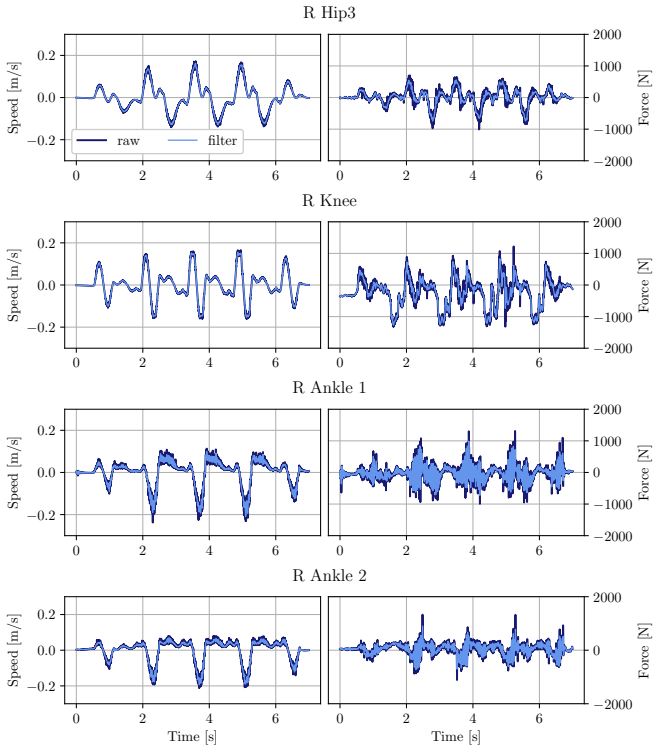

Fig. 6: Measured speed and effort for linear actuators in the fastest walking experiment (F3).

B. Step in place

In this experiment, the robot tried to perform the highest possible steps in the smallest amount of time. Starting with a step time of 1 s ($t_{ss} = 0.8$, $t_{ds} = 0.2$), the robot reached a maximum step height of 10 cm as shown in Fig. 7. After reducing the time to 0.75 s ($t_{ss} = 0.7$, $t_{ds} = 0.05$) the robot

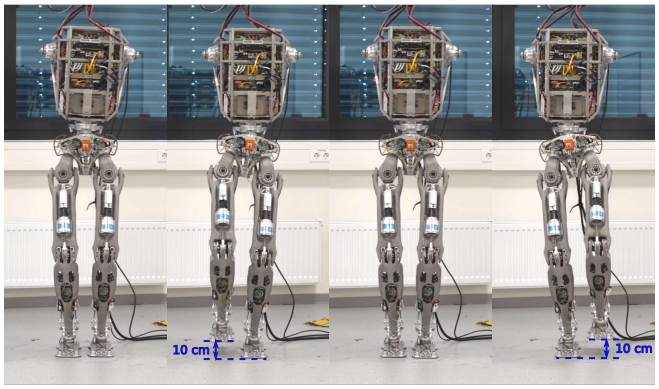

Fig. 7: Stepping in place experiment with a step height of 10 cm and a step time of 1 s.

TABLE VI: Overview of stepping in place experiments.

Time [s]	Step height [cm]				
	4	6	8	10	12
1.00	-	✓	✓	✓	✗
0.75	-	✓	✓	✗	-
0.70	✓	✓	✗	-	-

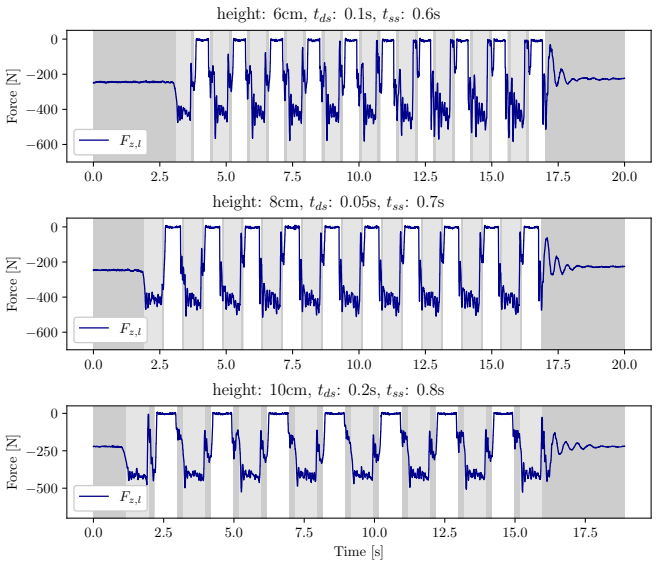

Fig. 8: Measured forces along z-axis of left and right F/Ts for stepping in place experiments at different heights and timings. Background is colored when in the desired trajectory one foot (light gray) or two feet (dark gray) are supposed to be in contact with the ground.

succeeded up to 8 cm step height. Finally, using a step time of 0.7 s ($t_{ss} = 0.6$, $t_{ds} = 0.1$), the maximum step height reached by the robot was 6 cm.

Table VI reports the obtained successes and failures. All the failures have been caused by triggering the velocity limit of knee actuators. Similarly to the fast walk experiment and as reported in Table IV, in successful experiments RH5 approached the velocity limit but used small effort. Consequently, a change in the actuator' screw pitch will easily improve the results.

As visible in Fig. 8, the measured contact forces remain consistent all along the duration of the experiment. Thanks to the compliance introduced by the Whole-body Controller, the behavior of RH5 does not diverge in case of small early contacts, which means that the robot is stable and not affected by undesired oscillations.

C. Long strides

In the last experiment, we tried to reach the maximum stride length that can be achieved by the RH5 robot with the presented control architecture. As pictured in Fig. 9 and documented in Fig. 10, the longest stride achieved by RH5 is 90 cm long while moving with a step time of 3.5 seconds.

The slower gait speed is a consequence of difficulties encountered in the feet touchdown phases. Because of early contact problems due to mechanical flexibility, we haven't been able to further reduce the step time. This resulted in a quasi-static motion, meaning that during each step the CoM ground projection falls close the anchor foot support area. To perform a stride of 0.9 m with such limitation on CoM position and considering a constant CoM height, RH5 almost reached the position limit for the ankle joints with the actuators close to being fully retracted. By improving the touchdown phases and therefore generating a faster and more dynamic motion, the ankle position issue will be reduced. With Optimal Control (OC), it would be possible to optimize a dynamically stable motion from start to end having minimal constraints on contact positions and initial/final configuration. Feet orientation after take off can be optimized automatically in such a way to reduce the maximum speed or used range of motion.

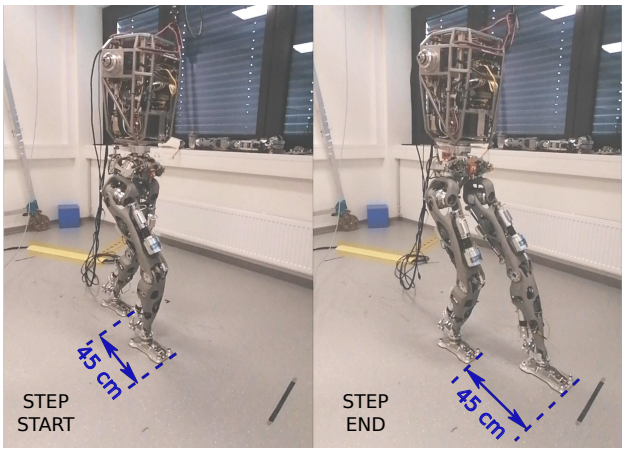

Fig. 9: RH5 robot executig the longest stride of 90 cm.

V. CONCLUSIONS

This paper presents an experimental analysis of dynamic walking capabilities of RH5 humanoid using ZMP motion planning and whole body control approaches. With ground truth motion capture data, it was shown that the robot is able to walk with a speed of 0.43 m/s which makes it one of the fastest walking humanoids with similar size and

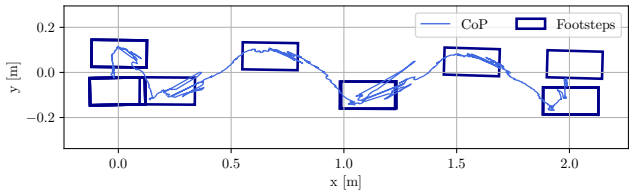

Fig. 10: Measured footsteps for long stride experiment with a stride length of 90 cm, t_{ss} of 2.0 s and t_{ds} of 1.5 s.

actuation capabilities. In addition, the robot can do fast in-place tapping motions as well as walking with long strides of up to 90 cm. Further, we identify the limitations of the robot design and propose easy to implement hardware modifications which will further help us boost its walking speed. In the near future, we plan to combine the upper body humanoid RH5 Manus with the improved RH5 lower body in order to achieve a more capable humanoid robot.

ACKNOWLEDGMENT

This research was done in the M-RoCK (FKZ 01IW21002), VeryHuman (FKZ 01IW20004) and KiMMI-SF (DFKI: 50RA2021, Uni: 50RA2022), projects funded by the German Aerospace Center (DLR) with federal funds from the Federal Ministry of Education and Research (BMBF) and from the Federal Ministry for Economic Affairs and Climate Action (BMWK).

REFERENCES

[1] M. Hirose and K. Ogawa, "Honda humanoid robots development," *Philosophical Transactions: Mathematical, Physical and Engineering Sciences*, vol. 365, no. 1850, pp. 11–19, 2007. [Online]. Available: http://www.jstor.org/stable/25190425

[2] B.-K. Cho, S.-S. Park, and J.-h. Oh, "Controllers for running in the humanoid robot, hubo," in *2009 9th IEEE-RAS International Conference on Humanoid Robots*, 2009, pp. 385–390.

[3] "Atlas, Boston Dynamics." https://www.bostondynamics.com/atlas, accessed: 2023-07-22.

[4] Y. Gong, R. Hartley, X. Da, A. Hereid, O. Harib, J.-K. Huang, and J. Grizzle, "Feedback control of a cassie bipedal robot: Walking, standing, and riding a segway," in *2019 American Control Conference (ACC)*, 2019, pp. 4559–4566.

[5] "Digit, Agility Robotics." https://robotsguide.com/robots/digit, accessed: 2023-07-22.

[6] T. Buschmann, V. Favot, S. Lohmeier, M. Schwienbacher, and H. Ulbrich, "Experiments in fast biped walking," in *2011 IEEE International Conference on Mechatronics*, 2011, pp. 863–868.

[7] T. Jung, J. Lim, H. Bae, K. K. Lee, H.-M. Joe, and J.-H. Oh, "Development of the humanoid disaster response platform drc-hubo+," *IEEE Transactions on Robotics*, vol. 34, no. 1, pp. 1–17, 2018.

[8] J. L. et al., "Robot system of DRC-HUBO+ and control strategy of team KAIST in DARPA robotics challenge finals," *Journal of Field Robotics*, vol. 34, no. 4, pp. 802–829, Sept. 2016. [Online]. Available: https://doi.org/10.1002/rob.21673

[9] G. Mesesan, J. Englsberger, G. Garofalo, C. Ott, and A. Albu-Schäffer, "Dynamic walking on compliant and uneven terrain using dcm and passivity-based whole-body control," in *IEEE-RAS International Conference on Humanoid Robots*, October 2019. [Online]. Available: https://elib.dlr.de/130765/

[10] R. Budhiraja, J. Carpentier, C. Mastalli, and N. Mansard, "Differential dynamic programming for multi-phase rigid contact dynamics," in *2018 IEEE-RAS 18th International Conference on Humanoid Robots (Humanoids)*, 2018, pp. 1–9.

[11] N. A. Villa, P. Fernbach, M. Naveau, G. Saurel, E. Dantec, N. Mansard, and O. Stasse, "Torque controlled locomotion of a biped robot with link flexibility," in *2022 IEEE-RAS 21st International Conference on Humanoid Robots (Humanoids)*, 2022, pp. 9–16.

[12] A. Yousefi-Koma, B. Maleki, H. Maleki, A. Amani, M. A. Bazrafshani, H. Keshavarz, A. Iranmanesh, A. Yazdanpanah, H. Alai, S. Salehi, M. Ashkvari, M. Mousavi, and M. S. Ashtiani, "Surenaiv: Towards a cost-effective full-size humanoid robot for real-world scenarios," in *2020 IEEE-RAS 20th International Conference on Humanoid Robots (Humanoids)*, 2021, pp. 142–148.

[13] I. Kumagai, R. Ueda, F. Sugai, S. Nozawa, Y. Kakiuchi, K. Okada, and M. Inaba, "Achievement of localization system for humanoid robots with virtual horizontal scan relative to improved odometry fusing internal sensors and visual information," in *2016 IEEE/RSJ International Conference on Intelligent Robots and Systems (IROS)*, 2016, pp. 666–673.

[14] V. Dimitrov, M. Wonsick, X. Long, P. Maurice, D. Sternad, and T. Padir, "Towards designing benchmarks for humanoid space robots: Northeastern's NASA valkyrie dataset." [Online]. Available: https://doi.org/10.22541%2Fau.158199808.87090372

[15] N. G. e. a. Tsagarakis, "Walk-man: A high-performance humanoid platform for realistic environments," *Journal of Field Robotics*, vol. 34, no. 7, pp. 1225–1259, 2017. [Online]. Available: https://onlinelibrary.wiley.com/doi/abs/10.1002/rob.21702

[16] J. Eßer, S. Kumar, H. Peters, V. Bargsten, J. de Gea Fernandez, C. Mastalli, O. Stasse, and F. Kirchner, "Design, analysis and control of the series-parallel hybrid rh5 humanoid robot," in *2020 IEEE-RAS 20th International Conference on Humanoid Robots (Humanoids)*. IEEE, 2021, pp. 400–407.

[17] M. Boukheddimi, S. Kumar, H. Peters, D. Mronga, R. Budhiraja, and F. Kirchner, "Introducing rh5 manus: A powerful humanoid upper body design for dynamic movements," in *2022 International Conference on Robotics and Automation (ICRA)*, 2022, pp. 01–07.

[18] M. Boukheddimi, R. Kumar, S. Kumar, J. Carpentier, and F. Kirchner, "Investigations into exploiting the full capabilities of a series-parallel hybrid humanoid using whole body trajectory optimization," in *2023 IEEE/RSJ International Conference on Intelligent Robots and Systems (IROS)*, 2023.

[19] M. Boukheddimi, D. Harnack, S. Kumar, R. Kumar, S. Vyas, O. Arriaga, and F. Kirchner, "Robot dance generation with music based trajectory optimization," in *2022 IEEE/RSJ International Conference on Intelligent Robots and Systems (IROS)*, 2022, pp. 3069–3076.

[20] R. Tedrake, S. Kuindersma, R. Deits, and K. Miura, "A closed-form solution for real-time zmp gait generation and feedback stabilization," in *2015 IEEE-RAS 15th International Conference on Humanoid Robots (Humanoids)*, 2015, pp. 936–940.

[21] S. Caron, A. Kheddar, and O. Tempier, "Stair climbing stabilization of the hrp-4 humanoid robot using whole-body admittance control," in *2019 International Conference on Robotics and Automation (ICRA)*, 2019, pp. 277–283.

[22] S. Kajita, H. Hirukawa, K. Harada, and K. Yokoi, *Introduction to Humanoid Robotics* -. Berlin, Heidelberg: Springer, 2014.

[23] S. Kajita, M. Morisawa, K. Miura, S. Nakaoka, K. Harada, K. Kaneko, F. Kanehiro, and K. Yokoi, "Biped walking stabilization based on linear inverted pendulum tracking," 11 2010, pp. 4489 – 4496.

[24] A. Del Prete, N. Mansard, O. Ramos, O. Stasse, and F. Nori, "Implementing torque control with high-ratio gear boxes and without joint-torque sensors," *International Journal of Humanoid Robotics*, vol. 13, 03 2015.

[25] D. Mronga, S. Kumar, and F. Kirchner, "Whole-body control of series-parallel hybrid robots," in *2022 International Conference on Robotics and Automation (ICRA)*. IEEE, 05 2022, pp. 228–234.

[26] S. Kumar, K. A. v. Szadkowski, A. Mueller, and F. Kirchner, "An Analytical and Modular Software Workbench for Solving Kinematics and Dynamics of Series-Parallel Hybrid Robots," *Journal of Mechanisms and Robotics*, vol. 12, no. 2, 02 2020, 021114. [Online]. Available: https://doi.org/10.1115/1.4045941

[27] R. Tedrake and the Drake Development Team, "Drake: Model-based design and verification for robotics," 2019. [Online]. Available: https://drake.mit.edu

[28] "ROCK, the Robot Construction Kit," http://www.rock-robotics.org.

[29] R. Cisneros, K. Yokoi, and E. Yoshida, "Yaw moment compensation by using full body motion," in *2014 IEEE International Conference on Mechatronics and Automation*, 2014, pp. 119–125.